Computer-Aided Analysis of Free-Running Microwave Oscillators

Chao-Ren Chang, Michael B. Steer, *Senior Member, IEEE*, Scott Martin, and Elias Reese, Jr., *Member, IEEE*

Abstract—**Traditionally, the design of microwave oscillators has been based on small-signal analysis techniques, which generally produced good results. However, large-signal simulations are often necessary to provide a more accurate characterization of oscillator performance. In this paper, an algorithm for free-runing oscillator analysis is presented. Kurokawa's oscillation condition is coupled with the modified nodal admittance form of the circuit equations to avoid degenerate solutions. The algorithm has been implemented using both harmonic balance and frequency-domain spectral balance techniques. The oscillator analysis was applied to the simulation of a monolithically integrated varactor-tuned MESFET oscillator. Good agreement between simulated power and oscillation frequency results and the measured data was obtained.**

I. Introduction

SMALL-SIGNAL analysis techniques form the basis of a systematic oscillator design procedure [1]–[3]. However, they do not yield power or harmonic content information. Large-signal simulation is necessary to provide this more accurate characterization of oscillator performance. This is particularly important in achieving a first-pass successful design of monolithic microwave integrated circuit (MMIC) VCO's. A successful design and analysis strategy is to determine a circuit topology early in the design phase using small-signal techniques. Then a large-signal analysis focuses on reliable performance predictions and subsequent optimization of the oscillator design.

Rizzoli *et al.* [4], [5] proposed a method (implemented in [6]) based on the harmonic balance technique for oscillator synthesis. The oscillation frequency is fixed while one circuit parameter is optimized to ensure that the harmonic balance equations are satisfied at that frequency. This method is numerically efficient and yields well-defined and accurate results. However, it is not directly amenable to free-running oscillator analysis as the frequency is fixed and a degree of freedom, such as a tuning element or the load impedance, is varied until harmonic balance is achieved. By repeating this process for a number of frequencies, a curve of frequency versus the degree of freedom is obtained. In this manner oscillators can be analyzed without involving autonomous circuit simulation.

The obvious approach to free-running oscillator analysis is to use the harmonic balance equations developed for the circuit and to include the oscillation frequency as an additional optimization variable. This method has been used by a number of workers [7], [8]. Generally, one of the variables that would be used as an optimization variable in examining a nonautonomous circuit[1] is eliminated, for example, by setting the phase of a voltage or current to zero. Usually, with this approach, the simulated results tend to converge to a degenerate solution [9] (e.g. all currents equal to zero is also a solution of Kirchhoff's current law, which is the basis of the harmonic balance equations), or else the initial setting of the oscillating frequency must be very close to the final result [8].

The degenerate solution can be avoided by incorporating additional criteria in the system objective function. This was done by Sterzer [10], in the early 1960's, in calculating the output power of a GaAs tunnel diode oscillator by incorporating the Kurokawa oscillation condition [11]. Also, in the early 1980's Solbach [12], working with a Gunn diode oscillator, and Bates [13], examining an IMPATT diode oscillator, predicted the frequency and output power by solving multifrequency forms of Kurokawa's oscillation condition [14] using frequency-domain power-series analysis techniques. However, the work on single-diode oscillator circuits cannot be directly extended to general nonlinear oscillator circuits. While not amenable to autonomous circuit simulation, the method of Rizzoli *et al.* uses a finite output power at the fundamental as an optimization criterion to avoid the degenerate solution.

Many workers have implemented noniterative nonlinear analyses of free-running oscillators using describing function techniques [15], [16] (commonly used in nonlinear control system analysis) and functional expansions

Manuscript received July 24, 1990; revised May 13, 1991. This work was supported in part by a National Science Foundation Presidential Young Investigator Award (Grant ECS-8657836) to M. B. Steer.

C.-R. Chang was with the Electrical and Computer Engineering Department, North Carolina State University, Raleigh. He is now with Compact Software, 483 McLean Boulevard, Paterson, NJ 07504.

M. B. Steer is with the Electrical and Computer Engineering Department, North Carolina State University, Raleigh, NC 27695-7911.

S. Martin and E. Reese, Jr. are with Texas Instruments, P.O. Box 655474, Dallas, TX 75265.

IEEE Log Number 9102327.

[1]A nonautonomous circuit is one in which the frequencies of signals are determined by signal sources. For example, an amplifier is a nonautonomous circuit.

0018-9480/91/1000-1735$01.00 ©1991 IEEE

(generally based on Volterra series techniques [17]–[19], but also using specialized functional expansions [20]). In these techniques, the system equations and oscillation criteria are combined to yield a set of algebraic equations which can be solved recursively. However, these methods are restricted to weakly nonlinear oscillators. Cheng and Everard [21] used a spectral balance approach to analyze a microwave FET oscillator. They used a Volterra series technique to generate the harmonic components, but since they used power series expansions of the nonlinear element characteristics, their technique is not restricted to weakly nonlinear oscillators. In their method they converted an oscillator into a one-port network by making a break somewhere in the circuit. This leads to the oscillation criterion whereby the impedance looking into this port is zero at the fundamental and at all harmonics. A relaxation algorithm is used to solve for this condition. The relaxation algorithm, however, has poor convergence properties and the use of Volterra-series-based nonlinear analysis is restrictive (limiting the analysis to one-dimensional nonlinearities and, unless power-series-like descriptions are available, to weakly nonlinear oscillators). This strategy of converting an oscillator into a one-port network also appears to have been implemented in a commercial nonlinear free-running oscillator simulator [22].

All of the above techniques assume that a periodic steady-state solution of the system equations exists and then proceed to derive it. In contrast, large-signal oscillator analysis in the time domain using programs such as SPICE [23] allows the buildup of oscillations to be observed [24]. In spite of the time required and the difficulty of determining the time at which steady state is obtained, time-domain simulation techniques have the ability to predict the start-up of oscillation in addition to the frequency of oscillation and non-steady-state behavior (e.g. chaotic behavior). It is also easier to incorporate physical device models (e.g. those described by coupled partial differential equations or electron statistics) in time-domain simulations [25]–[27].

The purpose of this paper is to present a newly developed free-running steady-state oscillator analysis algorithm suited to large-signal oscillator analysis. Either fourier-transform-based harmonic balance techniques or frequency-domain spectral balance techniques can be used for the nonlinear analyses, and strong nonlinearities are allowed. In the algorithm, the oscillating frequency is used as an independent variable and the system error function is modified to partially incorporate the Kurokawa oscillation criterion. The major contribution of the work reported here is formulating the problem so that the resulting set of equations can be solved using the Newton method to speed convergence. The method also has good convergence properties so that the initial setting of the frequency variable need not be very close to the actual oscillating frequency. In Section II, we first briefly describe the Kurokawa condition for steady-state oscillation since it is the theoretical base of the analysis algorithm. Then, in Sections II and III, the algorithm is developed and discussed. The algorithm developed here was implemented in the general-purpose simulator FREDA2 and was applied to the simulation of a varactor-tuned MESFET oscillator from Texas Instruments (part TI EG8132). In Sections IV and V, the design and characterization of the TI EG8132 are described and in Section VI, the simulated results and a discussion are presented.

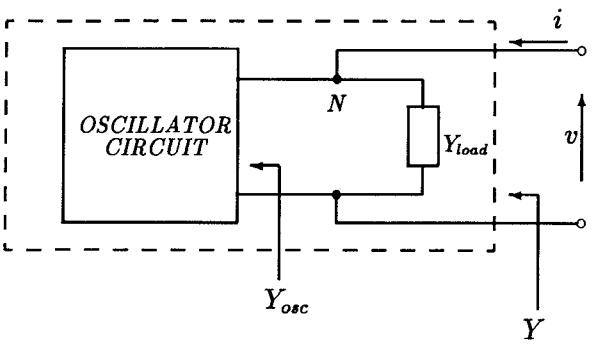

Fig. 1. One-port equivalent circuit of an oscillator circuit.

II. System Equations

The steady-state response of nonlinear microwave circuits is generally obtained using a Newton iteration scheme to solve a set of system equations expressed in the frequency domain. In [28], a set of nonlinear system equations for nonautonomous circuit analysis was developed, by applying Kirchhoff's laws, as

$$M(x)x = y \tag{1}$$

where the x-dependent circuit matrix $M(x)$ is a modified nodal admittance matrix; vector y represents the independent source vector; and x is the independent variable vector, which contains all the necessary node voltages and edge currents at various frequencies. Equation (1) is considerably reduced in size by partitioning the nonlinear system into linear and nonlinear subcircuits and using matrix reduction techniques on the linear subcircuit so that only the voltages and currents at the nodes common to the nonlinear subcircuit need be considered. While solution of (1) yields the steady-state response of nonautonomous circuits, this is not sufficient to determine the response of autonomous circuits, since generally the degenerate solution (i.e., with all ac voltages and ac currents zero) is preferred. Our approach is to expand the set of equations to partially include the Kurokawa oscillation condition [11], thereby ensuring that the degenerate solution is not obtained.

A free-running oscillator circuit can be treated as a one-port network by looking into the terminals of a load element Y_{load}, as shown in Fig. 1. Then the steady-state oscillation condition [11] (known as the Kurokawa condition) for a single frequency of oscillation can be expressed as

$$Y(\omega) = Y_{\text{osc}}(\omega) + Y_{\text{load}}(\omega) = 0 \tag{2}$$

where $Y(\omega)$ is the input admittance of the one-port net-

work, and $Y_{osc}(\omega)$ and $Y_{load}(\omega)$ are the equivalent admittances of the "oscillator circuit" and the load element respectively. Kurokawa derived (2) with a single frequency only. However, in general, harmonics of the voltages and currents will be present, and (2) also applies to each frequency component. Therefore, if K different ac frequency components are present, the condition for the oscillation of the circuit in Fig. 1 is [14].

$$Y_k = Y_{osc,k} + Y_{load,k} = \mathrm{Re}\{Y_k\} + j\,\mathrm{Im}\{Y_k\} = 0, \quad k = 1,2,\cdots,K. \tag{3}$$

In (3), the subscript k indicates that the admittance Y_k is evaluated at the radian frequency ω_k. That is, if i and v in fig. 1 are represented as summations of different frequency components i_k and v_k, respectively, in the frequency domain:

$$i(t) = \sum_{k=0}^{K} i_k(t) = \sum_{k=0}^{K} |I_k|\cos(\omega_k t + \phi_k) \tag{4}$$

and

$$v(t) = \sum_{k=0}^{K} v_k(t) = \sum_{k=0}^{K} |V_k|\cos(\omega_k t + \theta_k) \tag{5}$$

then the input admittance Y_k evaluated at the radian frequency ω_k is

$$Y_k = \frac{I_k}{V_k}. \tag{6}$$

For a one-port nonlinear system, such as a single-diode circuit, the solution of the multifrequency Kurokawa condition (3) is also a solution of the system equation (1), but the degenerate solution of (1) is avoided. Solution of (3) has been the approach generally used in the analysis of single-diode oscillators [10]–[13]. This method could be extended to arbitrary nonlinear circuits by applying (3) at every node in the circuit and for every frequency component. This prevents the voltage and current components at every ω_k from being zero, which may not be justified. Alternatively, (1) can be solved simultaneously with a partial Kurokawa condition to avoid the degenerate solution at the fundamental oscillation frequency only. That is, (1) can be solved in conjunction with

$$Y_1 = Y_{osc,1} + Y_{load,1} = \mathrm{Re}\{Y_1\} + j\,\mathrm{Im}\{Y_1\} = 0. \tag{7}$$

By separating the real and imaginary parts of Y_1, (7) can be written as

$$\mathrm{Re}\{Y_1\} = \mathrm{Re}\{I_1 / V_1\} = 0 \tag{8}$$

and

$$\mathrm{Im}\{Y_1\} = \mathrm{Im}\{I_1 / V_1\} = 0 \tag{9}$$

which imply that

$$\mathrm{Re}\{I_1\} = \mathrm{Im}\{I_1\} = 0 \tag{10}$$

and

$$|V_1| \neq 0. \tag{11}$$

As an additional variable, f_1, needs to be added for oscillator analysis, and since $\mathrm{Re}\{Y_1\}$ may be frequency independent, simultaneous solution of (9) with (1) is required to obtain a matrix equation that is well conditioned with respect to f_1. If the augmented set of equations is limited to this, the degenerate solution will still be preferred if $\mathrm{Im}\{Y_1\}$ is not dependent on V_1. Generally $\mathrm{Re}\{Y_1\}$ is then strongly dependent on V_1 so that the degenerate solution is avoided by also incorporating (8) in the augmented set of equations. Note that stable oscillations are obtained when the amplitude increases sufficiently to vary the driving point admittance of the nonlinear element so that $Y_1 = 0$. Solution of the augmented set of equations is discussed in Section III.

III. System Error Minimization Algorithm

The most efficient way to solve the augmented system equations is to cast the problem into the minimization of an objective function:

$$\boldsymbol{f}(\boldsymbol{x}) = \boldsymbol{M}(\boldsymbol{x})\boldsymbol{x} - \boldsymbol{y} \tag{12}$$

and use Newton's method to iteratively obtain the zero of this function. The iterative process of Newton's method applied to (12) is represented as

$${}^{j+1}\boldsymbol{x} = {}^{j}\boldsymbol{x} - \boldsymbol{J}^{-1}({}^{j}\boldsymbol{x})\boldsymbol{f}({}^{j}\boldsymbol{x}) \tag{13}$$

where ${}^{j}\boldsymbol{x}$ is the independent variable vector at the jth iteration, $\boldsymbol{J}$ is the Jacobian matrix of $\boldsymbol{f}$, and $\boldsymbol{J}^{-1}$ is its inverse. For nonautonomous circuit analysis, vector $\boldsymbol{x}$ is composed of the node voltages and edge currents, and is structured as

$$\boldsymbol{x} = \left[\boldsymbol{x}_0^T \boldsymbol{x}_1^T \cdots \boldsymbol{x}_k^T \cdots \boldsymbol{x}_K^T\right]^T \tag{14}$$

where $\boldsymbol{x}_k$ is a subvector of $\boldsymbol{x}$ at the particular radian frequency ω_k. Similarly, vector $\boldsymbol{f}({}^{j}\boldsymbol{x})$ is composed of the elements of the difference vector between the independent source vector $\boldsymbol{y}$ and the induced source vector $\boldsymbol{y}({}^{j}\boldsymbol{x}) = \boldsymbol{M}({}^{j}\boldsymbol{x}){}^{j}\boldsymbol{x}$, and has the same structure as $\boldsymbol{x}$ in (14):

$$\boldsymbol{f}({}^{j}\boldsymbol{x}) = \left[\boldsymbol{f}_0^T({}^{j}\boldsymbol{x}) \quad \boldsymbol{f}_1^T({}^{j}\boldsymbol{x}) \cdots \boldsymbol{f}_k^T({}^{j}\boldsymbol{x}) \cdots \boldsymbol{f}_K^T({}^{j}\boldsymbol{x})\right]^T. \tag{15}$$

If $P+1$ node voltages and $Q+1$ edge currents are selected as independent variables and, for efficient calculation, complex elements in $\boldsymbol{x}$ and $\boldsymbol{f}({}^{j}\boldsymbol{x})$ are separated into real and imaginary parts, the structures of the subvector $\boldsymbol{x}_k$ and $\boldsymbol{f}_k({}^{j}\boldsymbol{x})$ for $k \neq 0$ are

$$\boldsymbol{x}_k = \left[V_{0,k,r} \quad V_{0,k,i} \quad V_{1,k,r} \quad V_{1,k,i} \cdots V_{P,k,r} \quad V_{P,k,i} \quad I_{0,k,r} \quad I_{0,k,i} \cdots I_{Q,k,r} \quad I_{Q,k,i}\right]^T \tag{16}$$

and

$$\boldsymbol{f}_k({}^{j}\boldsymbol{x}) = \left[J_{0,k,r}({}^{j}\boldsymbol{x}) \quad J_{0,k,i}({}^{j}\boldsymbol{x}) \quad J_{1,k,r}({}^{j}\boldsymbol{x}) \quad J_{1,k,i}({}^{j}\boldsymbol{x}) \cdots J_{P,k,r}({}^{j}\boldsymbol{x}) \quad J_{P,k,i}({}^{j}\boldsymbol{x}) \quad E_{0,k,r}({}^{j}\boldsymbol{x}) \quad E_{0,k,i}({}^{j}\boldsymbol{x}) \cdots E_{Q,k,r}({}^{j}\boldsymbol{x}) \quad E_{Q,k,i}({}^{j}\boldsymbol{x})\right]^T \tag{17}$$

respectively, where the variable voltage (or current) phasor at node n and radian frequency ω_k is $V_{n,k} = V_{n,k,r} + jV_{n,k,i}$ (or $I_{n,k} = I_{n,k,r} + jI_{n,k,i}$); the source current (or voltage) phasor $J_{n,k}$ (or $E_{n,k}$) is similarly defined.

For oscillator circuit analysis, the structure of $\boldsymbol{x}_1$ has to be changed, as the fundamental frequency, f_1, is an additional variable. Here the imaginary part of the fundamental voltage at node N (shown in Fig. 1) in (16) is replaced by f_1 (and so the phases of node voltages are referred to the phase of the edge voltage of the load element). Placing the node voltage of the load element in the first position of (16), the subvector $\boldsymbol{x}_1$ in (14) for oscillator analysis is constructed as

$$\boldsymbol{x}_1 = \left[V_{0,1,r} \quad f_1 \quad V_{1,1,r} \quad V_{1,1,i} \cdots V_{P,1,r} \quad V_{P,1,i} \quad I_{0,1,r} \quad I_{0,1,i} \cdots I_{Q,1,r} \quad I_{Q,1,i}\right]^T. \tag{18}$$

Likewise, the subvector $\boldsymbol{f}_1({}^j\boldsymbol{x})$ in (15) is reorganized by replacing the element $J_{0,1,i}({}^j\boldsymbol{x})$ in $\boldsymbol{f}_1({}^j\boldsymbol{x})$ (corresponding to the variable f_1 in $\boldsymbol{x}_1$) with $\mathrm{Im}\{Y_1\}$ from (9), and by replacing the element $J_{0,1,r}({}^j\boldsymbol{x})$ in $\boldsymbol{f}_1({}^j\boldsymbol{x})$ (corresponding to the variable f_1 in $\boldsymbol{x}_1$) with $\mathrm{Re}\{Y_1\}$ from (8):

$$\begin{aligned}\boldsymbol{f}_1({}^j\boldsymbol{x}) = \big[&\mathrm{Re}\{Y_1({}^j\boldsymbol{x})\} \quad \mathrm{Im}\{Y_1({}^j\boldsymbol{x})\} \quad J_{1,1,r}({}^j\boldsymbol{x}) \\ &J_{1,1,i}({}^j\boldsymbol{x}) \cdots J_{P,1,r}({}^j\boldsymbol{x}) \quad J_{P,1,i}({}^j\boldsymbol{x}) \\ &E_{0,1,r}({}^j\boldsymbol{x}) \quad E_{0,1,i}({}^j\boldsymbol{x}) \\ &\cdots E_{Q,1,r}({}^j\boldsymbol{x}) \quad E_{Q,1,i}({}^j\boldsymbol{x})\big]^T.\end{aligned} \tag{19}$$

A. Formulation of the Jacobian Matrix

The Jacobian matrix $\boldsymbol{J}({}^j\boldsymbol{x})$ is composed of $(K+1)\times(K+1)$ different blocks:

$$\boldsymbol{J}({}^j\boldsymbol{x}) = \begin{bmatrix} \boldsymbol{J}_{0,0}({}^j\boldsymbol{x}) & \boldsymbol{J}_{0,1}({}^j\boldsymbol{x}) & \cdots & \boldsymbol{J}_{0,K}({}^j\boldsymbol{x}) \\ \boldsymbol{J}_{1,0}({}^j\boldsymbol{x}) & \boldsymbol{J}_{1,1}({}^j\boldsymbol{x}) & \cdots & \boldsymbol{J}_{1,K}({}^j\boldsymbol{x}) \\ \vdots & \vdots & \cdots & \vdots \\ \boldsymbol{J}_{K,0}({}^j\boldsymbol{x}) & \boldsymbol{J}_{K,1}({}^j\boldsymbol{x}) & \cdots & \boldsymbol{J}_{K,K}({}^j\boldsymbol{x}) \end{bmatrix}. \tag{20}$$

Each block matrix $\boldsymbol{J}_{q,k}({}^j\boldsymbol{x})$ represents the block Jacobian matrix for input frequency ω_k and output frequency ω_q, and its elements are all possible derivatives of the functions in $\boldsymbol{f}_q({}^j\boldsymbol{x})$ with respect to the variables in $\boldsymbol{x}_k$. Except for $q=1$ or $k=1$, the structure of $\boldsymbol{J}_{q,k}$ is the same as that for nonautonomous circuit analysis [28]. The only difference is that some elements of $\boldsymbol{J}_{q,k}$ for $q=1$ or $k=1$ are replaced by derivatives of voltages and currents with respect to f_1, by derivatives of $\mathrm{Re}\{Y_1\}$, or by derivatives of $\mathrm{Im}\{Y_1\}$. In the following, equations for calculating the f_1, $\mathrm{Re}\{Y_1\}$, or $\mathrm{Im}\{Y_1\}$ related derivatives are presented.

Let $J_{n,k,s}({}^j\boldsymbol{x})$ represent elements of $\boldsymbol{f}({}^j\boldsymbol{x})$ at node n and radian frequency ω_k, where $s=r$ or i indicates the real or the imaginary part respectively. With the circuit separated into linear and nonlinear subcircuits, $J_{n,k,s}({}^j\boldsymbol{x})$ can be expressed as

$$J_{n,k,s}({}^j\boldsymbol{x}) = J_{L(n,k,s)}({}^j\boldsymbol{x}) + J_{NL(n,k,s)}({}^j\boldsymbol{x}) \tag{21}$$

where $J_{L(n,k,s)}({}^j\boldsymbol{x})$ and $J_{NL(n,k,s)}({}^j\boldsymbol{x})$ are the induced currents flowing into linear and nonlinear subcircuits from node n, respectively.

For the linear subcircuit, the derivatives $\partial J_{L(n,k,s)}({}^j\boldsymbol{x})/\partial f_1$ are calculated numerically using the secant method [29]. The linear portion of the system equation (1) can be extracted to calculate the linear current $J_{L(n,k,s)}({}^j\boldsymbol{x})$ at ω_k:

$$M^l_{ID(k,k)}\boldsymbol{x}_k = \boldsymbol{y}_{L(k)}({}^j\boldsymbol{x}), \qquad k=1,2,\cdots,K \tag{22}$$

where $M_{ID(k,k)}$ is the linear part of the diagonal block matrix $M_{k,k}({}^j\boldsymbol{x})$ of the modified nodal admittance matrix $\boldsymbol{M}({}^j\boldsymbol{x})$ at ω_k and is a function of ω_k; frequency f_k is not included in ${}^j\boldsymbol{x}_k$; and $J_{L(n,k,s)}({}^j\boldsymbol{x})$ are elements of $\boldsymbol{y}_{L(k)}({}^j\boldsymbol{x})$. Indeed $M_{ID(k,k)}$, $k=1,\cdots,K$, is the entire linear portion of $\boldsymbol{M}({}^j\boldsymbol{x})$, as linear components do not contribute to frequency conversion represented by $\boldsymbol{M}_{q,k}({}^j\boldsymbol{x})$, $q \neq k$. After calculating the derivatives $\partial J_{L(n,k,s)}({}^j\boldsymbol{x})/\partial f_k$ $(k=1,\cdots,K)$ by applying the secant method to (22), the derivatives $\partial J_{L(n,k,s)}({}^j\boldsymbol{x})/\partial f_1$ $(k=1,\cdots,K)$ which are required in the Jacobian matrix can be obtained as

$$\partial J_{L(n,k,s)}({}^j\boldsymbol{x})/\partial f_1 = k\left[\partial J_{L(n,k,s)}({}^j\boldsymbol{x})/\partial f_k\right]. \tag{23}$$

The contributions $\partial J_{NL(n,k,s)}({}^j\boldsymbol{x})/\partial f_1$ from the nonlinear subcircuit are calculated for each element. If the nonlinear element is a resistor, voltage-to-current transducer, or any other frequency-independent element, any derivatives with respect to f_1 for that element should be zero. However, for a nonlinear capacitor,

$$\partial J_{NL(n,k,s)}({}^j\boldsymbol{x})/\partial f_1 = J_{NL(n,k,s)}({}^j\boldsymbol{x})/f_1 \tag{24}$$

and, for a nonlinear inductor,

$$\partial J_{NL(n,k,s)}({}^j\boldsymbol{x})/\partial f_1 = -J_{NL(n,k,s)}({}^j\boldsymbol{x})/f_1. \tag{25}$$

In addition to the derivatives $\partial J_{n,k,s}({}^j\boldsymbol{x})/\partial f_1$, some $\mathrm{Re}\{Y_1\}$ and $\mathrm{Im}\{Y_1\}$ related derivatives, such as $\partial\,\mathrm{Im}\{Y_1\}/\partial V_{n,k,s}$ or $\partial\,\mathrm{Im}\{Y_1\}/\partial f_1$, are also required. These derivatives can be obtained from the previously calculated derivatives:

$$\begin{aligned}\partial\,\mathrm{Re}\{Y_1\}/\partial V_{n,k,s} &= \mathrm{Re}\left\{\frac{\partial Y_1}{\partial V_{n,k,s}}\right\} \\ &= \mathrm{Re}\left\{I_1\frac{\partial(1/V_1)}{\partial V_{n,k,s}} + (1/V_1)\frac{\partial I_1}{\partial V_{n,k,s}}\right\}\end{aligned} \tag{26}$$

$$\begin{aligned}\partial\,\mathrm{Im}\{Y_1\}/\partial V_{n,k,s} &= \mathrm{Im}\left\{\frac{\partial Y_1}{\partial V_{n,k,s}}\right\} \\ &= \mathrm{Im}\left\{I_1\frac{\partial(1/V_1)}{\partial V_{n,k,s}} + (1/V_1)\frac{\partial I_1}{\partial V_{n,k,s}}\right\}\end{aligned} \tag{27}$$

$$\partial\,\mathrm{Re}\{Y_1\}/\partial f_1 = \mathrm{Re}\left\{\frac{\partial Y_1}{\partial f_1}\right\} = \mathrm{Re}\left\{(1/V_1)\frac{\partial I_1}{\partial f_1}\right\} \tag{28}$$

and

$$\partial \operatorname{Im}\{Y_1\}/\partial f_1 = \operatorname{Im}\left\{\frac{\partial Y_1}{\partial f_1}\right\} = \operatorname{Im}\left\{(1/V_1)\frac{\partial I_1}{\partial f_1}\right\} \quad (29)$$

where $V_{n,k,s}$ is the node voltage defined in (16); I_1 and V_1 are complex numbers defined in (4) and (5), respectively; and

$$I_1({}^j\boldsymbol{x}) = J_{0,1,r}({}^j\boldsymbol{x}) + jJ_{0,1,i}({}^j\boldsymbol{x}). \quad (30)$$

Independent variables in the system equations include not only the node voltages and the oscillating frequency but also the edge currents. Derivatives with respect to the current variables can be calculated using procedures similar to those presented in this subsection.

B. Convergence Considerations

In oscillator circuit analyses, the convergence problem is even more troublesome than in nonautonomous circuit simulation. One of the reasons is that, in most oscillator circuits, the active device always operates in a large-signal condition. In nonautonomous circuit analyses, improved convergence under large-signal conditions can be achieved by sweeping the source signal from a low level to the desired level—the so-called continuation method. However, in oscillator circuit analysis the large-signal oscillation condition needs to be simulated directly. Furthermore, microwave circuits are generally designed with high-Q resonant tank circuits so that near the oscillation frequency the system error (e.g. the Kirchhoff's current law error) can be very large. In the following, two special techniques, *initial frequency setting* and *fundamental frequency searching*, that improve the convergence properties of oscillator circuit simulation are presented.

1) Initial Frequency Setting: The initial values chosen for the independent variables $\boldsymbol{x}_1$ in (18) strongly affect convergence properties. Generally speaking, all the node voltages and edge currents in $\boldsymbol{x}_1$ can be randomly initialized within a certain range which can reflect the practical oscillator output power level (typically, 0–20 dBm), and the oscillating frequency f_1 should not be initialized too far from the actual value. Our experience has shown that, for an oscillator circuit having the fundamental frequency f_{osc}, if f_1 is initialized between 0.1 f_{osc} and 10 f_{osc}, there is a good chance of converging to a solution.

It is recommended that several different initial f_1 values be tried until a solution is acquired, since there are so many factors (e.g. both I_1 and V_1 in (9) converging to low levels) which will cause convergence failure. In the minimization algorithm used here, after an estimated fundamental oscillating frequency range is given (such as from f_{low} to f_{high} in Fig. 2), the estimated frequency range is divided into 30 segments equally spaced logarithmically. In the circuit analysis, the first initial value of f_1 is set to be the center point, f_a, in Fig. 2. If convergence fails, for whatever reason, the simulation will automatically restart by resetting the initial value of f_1 to f_b. Then, the next one is set to f_c. This process continues until convergence is obtained or the initial frequency has shifted to the ends of the frequency range.

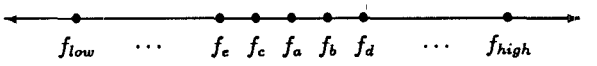

Fig. 2. The sequence of the initial fundamental frequency settings.

It should be noted that the estimated frequency range (from f_{low} to f_{high} in Fig. 2) is for initializing f_1 only. Once an initial value of f_1 is set and the Newton iterative procedure is in process, the required updated value of f_1 is not restricted to this range. Also, the initial value of f_1 need not be very close to the actual oscillating frequency. Starting with an initial guess of 5 GHz and converging to an actual operating frequency of 10 GHz is a common situation. However, choosing f_1 closer to the actual oscillation frequency has little effect on simulation time.

2) Fundamental Frequency Searching: Since most oscillator circuits operate under large-signal conditions and the active device is generally strongly nonlinear, the error surface for the oscillator analysis formulated in the vector $\boldsymbol{f}$ is much more complicated than that for nonautonomous circuit analyses. Therefore, another way of improving the convergence ability is to first decrease the number of harmonics so as to simplify the error surface and then restore it to the desired value gradually. In our implementation of oscillator analysis, we first consider the fundamental frequency and, when convergence has been obtained, repeat the analysis with the second-harmonic signal present. After repeating this process and obtaining the convergence with the third-harmonic signal present, the number of harmonics is then increased to the maximum number specified by the user. Note that if a Fourier-transform-based harmonic balance method is used, it is important to use oversampling to avoid aliasing [30] when a small number of frequency components are used.

IV. Oscillator Design

A Ku-band GaAs MMIC dual-varactor tuned FET oscillator was experimentally characterized and used to provide experimental verification of the oscillator nonlinear analysis technique. The design of the oscillator is described in [31], and the layout and schematics are shown in Figs. 3 and 4. The bias networks were designed to present broad-band open circuits to the FET so that the bias voltages were applied directly to the FET. The drain matching network was designed to transform the 50 Ω characteristic impedance of the output microstrip line so that a constant 15 Ω was presented to the drain of the MESFET. Broad-band coverage was obtained by first sweeping the reverse bias voltage on the varactor diode in the source leg and then sweeping the reverse bias voltage on the varactor diode in the gate leg. Thus, first decreasing impedances were presented to the source of the FET and then decreasing impedances were presented to the gate. The linear circuitry was designed so that optimum

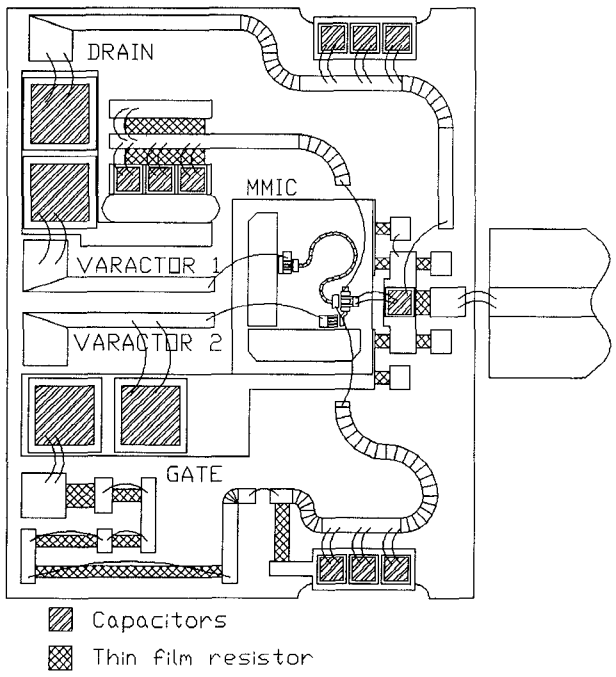

Fig. 3. Device layout of the TI EG8132 GaAs varactor-tuned FET oscillator.

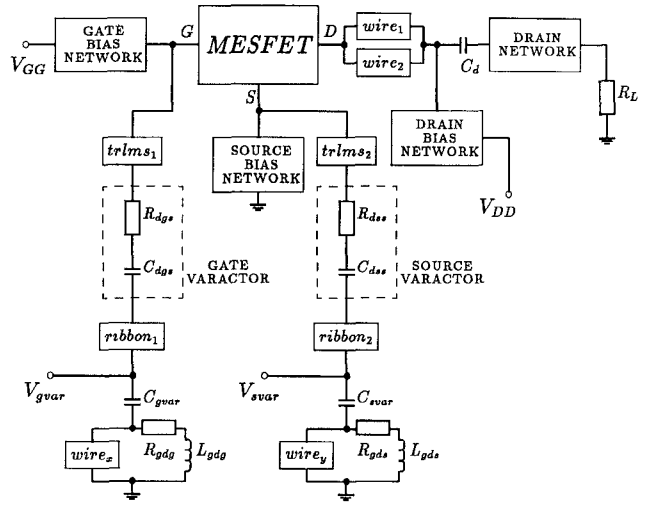

Fig. 4. Schematic of the TI EG8132 GaAs varactor-tuned FET oscillator. The *ribbon* and *wire* elements were modeled by a resistor and inductor in series. The *trlms* element is a microstrip transmission line.

source and gate impedances were presented at the low end of the tuning range and also at the high end. A unique varactor structure, detailed in [31], was realized to maintain high Q of the varactor diodes at large reverse biases. This avoided a frequency hole initially observed at intermediate tuning voltages using a conventional varactor structure. Assuming that the bias networks are ideal, the oscillator is modeled by about 35 linear elements in addition to the active devices. Including the bias networks, the oscillator is modeled by about 100 linear elements.

TABLE I
PARAMETER VALUES OF THE GATE AND SOURCE VARACTOR MODELS IN THE TI EG8132 OSCILLATOR

	Gate Varactor	Source Varactor
b	-8.0 V	-6.0 V
a_0	-0.54×10^{-12}	-0.09×10^{-12}
a_2	2.3×10^{-9}	4.783×10^{-10}
a_3	-8.7938×10^{-8}	-1.4703×10^{-8}
a_4	1.4×10^{-6}	1.8351×10^{-7}
a_5	-1.0458×10^{-5}	-1.0475×10^{-6}
a_6	3.048×10^{-5}	2.3177×10^{-6}

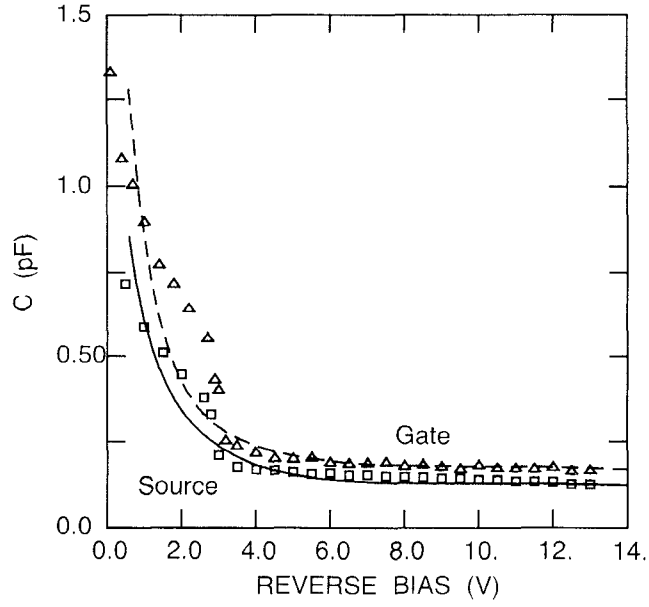

Fig. 5. The calculated equivalent capacitances (curves) from the models and the measured data (points) for both gate and source varactors of the TI EG8132 oscillator.

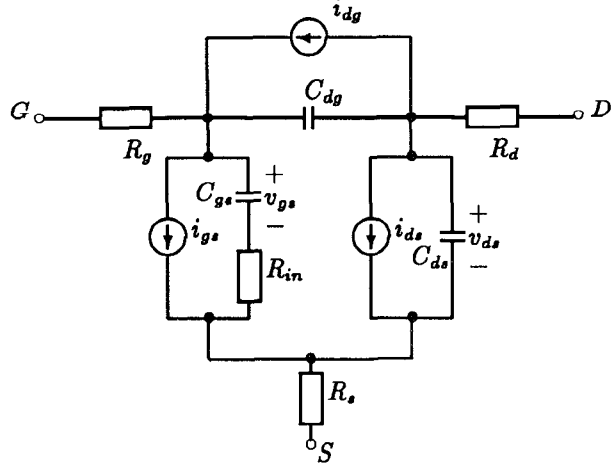

Fig. 6. Equivalent circuit of the MESFET of the TI EG8132 oscillator.

TABLE II
PARAMETER VALUES OF THE MESFET MODEL IN THE TI EG8132 OSCILLATOR

Parameter	Value
A_0	0.0698
A_1	0.0291
A_2	−0.00183
A_3	−0.00132
γ	1.632
β	0.0684
V_{ds}^0	3.0 V
τ	6.0×10^{-12}
I_0	1.0×10^{-9} A
η	7.0
V_R	20 V

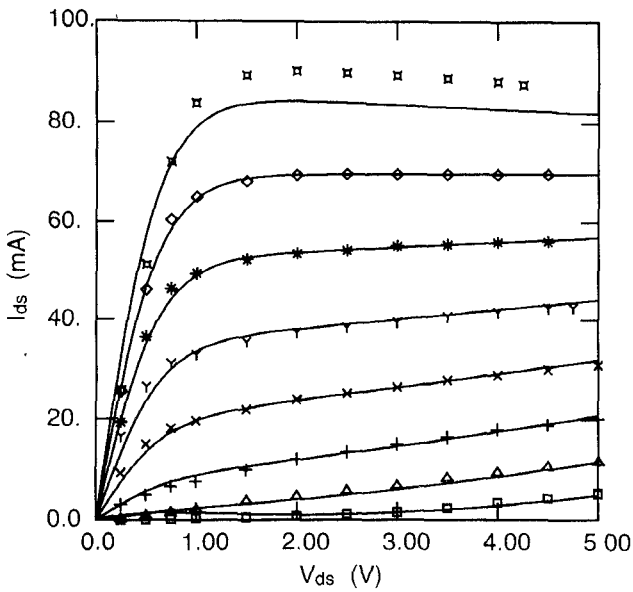

Fig. 7. The calculated i_{ds} (curves) from the MESFET model as a function of v_{ds} at $v_{gs} = -3$, -2.5, -2, -1.5, -1, -0.5, 0, and 0.5 V. Points are the measured data.

V. ACTIVE DEVICE CHARACTERIZATION

Each varactor diode was modeled as series-connected resistor and nonlinear capacitor. The capacitances, the major frequency tuning factors, were modeled to fit the measured data using a negative-ordered power series:

$$C = a_0 + a_2(V-b)^{-2} + a_3(V-b)^{-3} + \cdots + a_6(V-b)^{-6}. \quad (31)$$

Here V is the applied reverse bias voltage, and a and b are constants. This equation was fitted to measurements using a least-squares technique yielding the parameter values listed in Table I. The capacitances calculated using the model are compared with the measured data in Fig. 5.

The MESFET was modeled using the equivalent circuit shown in Fig. 6, which is similar to the one used in the Curtice model [32]. The only difference is that the element R_{ds}, which is an individual element in the Curtice model, is merged with the drain–source current generator, i_{ds}. The nonlinear elements of the model are defined as

$$i_{gs} = I_0\left(e^{v_{gs}/(\eta V_T)} - 1\right) \quad (32)$$

$$i_{dg} = I_0\left(e^{(v_{dg}-V_R)/V_T} + 1\right) \quad (33)$$

and

$$i_{ds} = \left(A_0 + A_1 v_1 + A_2 v_1^2 + A_3 v_1^3\right)\tanh(\gamma v_{ds}), \quad (34)$$

where

$$v_1 = v_{gs}(t-\tau)\left[1+\beta\left(V_{ds}^0 - v_{ds}\right)\right]. \quad (35)$$

Table II lists all the parameter values of (32)–(35). The calculated i_{ds} curves using model (34) and (35) are compared with the measured data in Fig. 7. A simplified circuit diagram is shown in Fig. 4.

VI. SIMULATION RESULTS AND DISCUSSION

The oscillator analysis algorithm was implemented in the microwave analog circuit simulator FREDA2 [28], [30], [33]. Linear elements are analyzed using the modified nodal admittance matrix, and the nonlinear elements are analyzed using the arithmetic operator method (AOM)—a frequency-domain spectral balance method [33] or the discrete-Fourier-transform-based harmonic balance method similar to that described in [34]. This program was used to investigate the TI EG8132 VCO from Texas Instruments. This VCO was previously analyzed using the method of Rizzoli *et al.* [35], [36].

In the first simulation to be presented, the gate, source, and drain bias networks were treated as ideal—presenting open circuits to the MESFET at all frequencies but dc, when the external bias voltages were applied directly to the MESFET. The dashed curve in Fig. 8 shows the simulated fundamental oscillation frequency with respect to the total tuning voltage, V_T (the sum of the gate and source tuning voltages), applied to the gate and source varactor diodes. The points are measured data and the solid line is the result using the complete circuit (including the actual bias networks). During the simulation, the tuning voltage is applied to the source varactor first. After the reverse bias of the source varactor has changed from 1 V to 13 V, the reverse bias of the gate varactor increases from 0 V to 15 V. The predicted frequency curve without the bias networks is closer to the measured data.

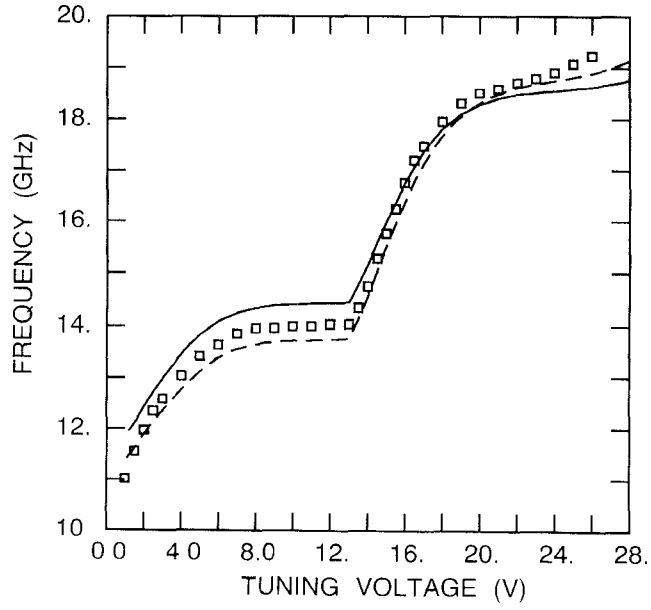

Fig. 8. The simulated fundamental oscillation frequency versus the total tuning voltage, V_T. Solid line is for the complete oscillator circuit; dashed line is for the core circuit; and points are measured data.

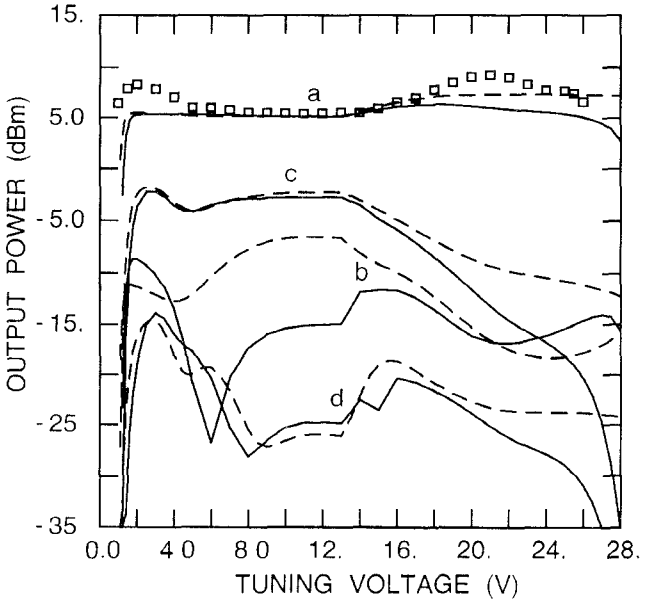

Fig. 9. The simulated output power at the fundamental frequency (*a*) and at the second (*b*), third (*c*), and fourth (*d*) harmonics. Solid lines are for the complete oscillator circuit, dashed lines are for the circuit with ideal bias networks, and points are measured data.

However, both results deviate less than 500 MHz ($< 3\%$) from the measured data.

Fig. 9 shows the simulated output power delivered to the 50 Ω microstrip output line at the fundamental and at the second, third, and fourth harmonic frequencies. As before, solid lines and dashed lines are for the complete circuit and the circuit with ideal bias networks, respectively. The points are measured output power at the fundamental frequency. The results obtained using the Fourier-transform-based harmonic balance method in the nonlinear analysis were virtually identical to those obtained using the frequency-domain spectral balance method. From Fig. 9, the oscillation tuning range can be accurately predicted. Although, because of the modeling inaccuracy, some differences have been shown in both Figs. 8 and 9 between the predicted values and the measured data, in general good agreement is seen. Most of the discrepancy is due to modeling inaccuracy, particularly the modeling of the MESFET at the waveform extremities—(low I_{ds}, high V_{ds}) and (high I_{ds}, low V_{ds})—and the modeling of bond wires and ribbons.

Simulated results in Figs. 8 and 9 were performed by sweeping the reverse biases of the source and gate varactors, in turn, in 0.5 V steps beginning with a 13 V tuning voltage—the middle of the range of oscillation. While sweeping the parameter values during the simulation, the previous results were used as the initial guesses for the next simulation. Convergence, in this case, was easily obtained. However, for the first simulation, the initial frequency guessed was arbitrary. Several different initial frequency settings were needed to obtain convergence. On average, with seven ac frequencies considered and using the AOM for the nonlinear analysis, the computer CPU time required to simulate the VCO with ideal bias networks was about 105 s per point in Figs. 8 and 9, and the CPU time required for the simulation of the complete circuit was about 17 min per point. The times were measured on a DEC DS3100 RISC workstation (rated at 12-13 VAX 11/780 MIPS) and the convergence criteria were 100 nA total Kirchhoff's current law error and $\mathrm{Re}\{Y_1\}, \mathrm{Im}\{Y_1\} < 100$ nS. Seven harmonics were included in the simulation, with the seventh harmonic approximately 40 dB below the fundamental. For the complete circuit simulation, most of the CPU time is consumed in the computations for the linear elements, since the nodal admittance matrix for the linear elements has to be recalculated after each iteration as the frequency is updated.

The oscillation tuning range is accurately predicted as shown in Fig. 9. The rapid drop-off in power at the extremes of V_T is principally due to drops in the Q's of the varactor diodes. The power peaking at low and high V_T is primarily due to the variations of the source and gate varactor impedances since at low V_T the source varactor impedance is optimum for maximum power transfer to the load. Similarly the gate varactor impedance is optimum at large V_T. The power peaking was investigated by plotting the drain–source i–v characteristics at various tuning voltages. Three characteristics are shown in Figs. 10–12 at V_T's of 3 V, 10 V, and 21 V, corresponding to the power peak at low V_T, the low-power flat region at intermediate V_T, and the power peak at large V_T, respectively. At $V_T = 3$ V the reverse bias voltages across the source and gate varactors are 3 V and 0 V, respectively, and the fundamentals of the drain–source current and voltage are approximately in phase, as indicated by the closed i–v locus in Fig. 10. Thus there is close to maximum power transfer to the load. Also the origins of the strong harmonics at low V_T can be seen in the low I_{ds} and high V_{ds} regions. At $V_T = 10$ V the source

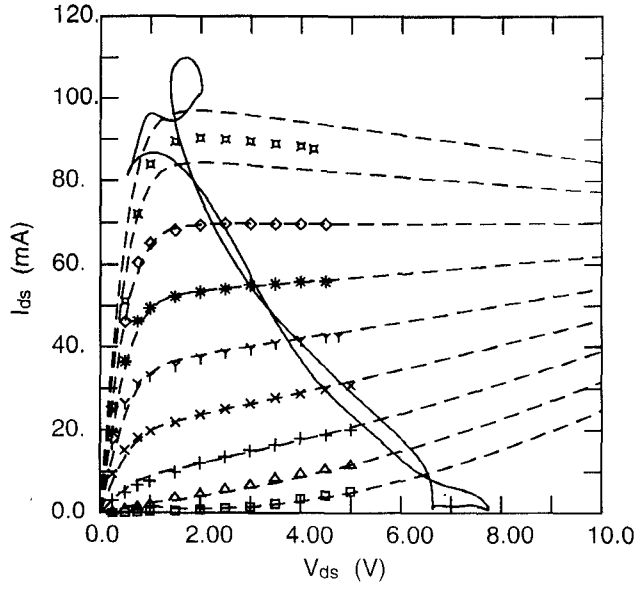

Fig. 10. The simulated i_{ds} versus v_{ds} locus at $V_T = 3$ V, where the reverse voltages across the gate and source varactors are 0 V and 3 V, respectively.

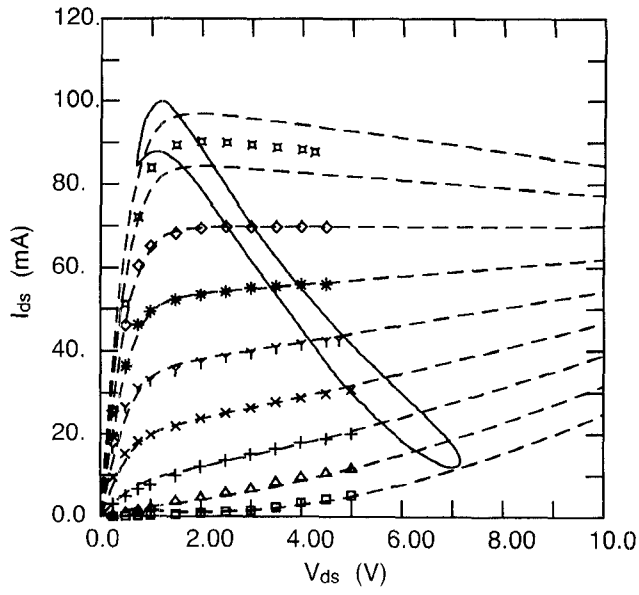

Fig. 12. The simulated i_{ds} versus v_{ds} locus at $V_T = 21$ V, where the reverse voltages across the gate and source varactors are 8 V and 13 V, respectively.

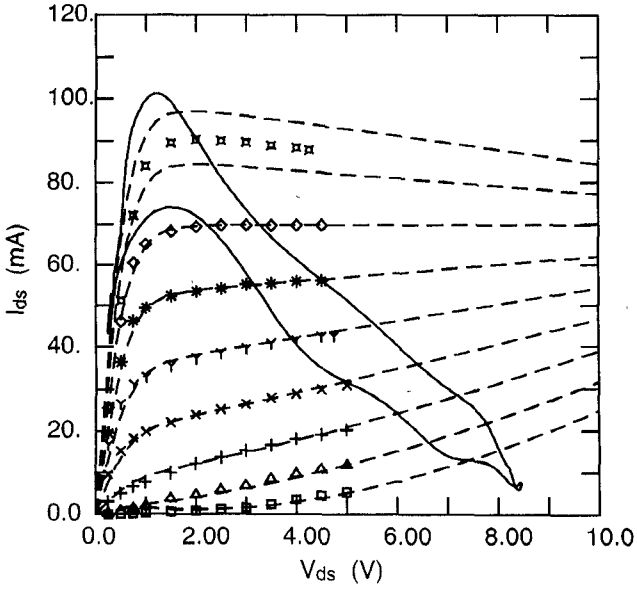

Fig. 11. The simulated i_{ds} versus v_{ds} locus at $V_T = 10$ V, where the reverse voltages across the gate and source varactors are 0 V and 10 V, respectively.

and gate varactors have 10 V and 0 V reverse bias voltages. The source impedance has changed significantly while the gate impedance is virtually unchanged. The fundamental drain–source current and voltage are no longer in phase, as indicated by the opening of the $i-v$ locus in Fig. 11. In this case power is not efficiently transferred to the load. With 13 V and 8 V reverse biases across the source and gate varactors, respectively, (i.e., at $V_T = 21$ V), nearly optimum impedances are again presented to the gate and source terminals of the MESFET. Now the fundamental I_{ds} and V_{ds} are almost in phase, as can be seen in Fig. 12. The discrepancy in the simulated and measured peak oscillation powers is thought to be due to inadequacies in modeling the MESFET in the low I_{ds}/high V_{ds} and the low V_{DS}/high I_{DS} regions, and in modeling the Q's of the varactor diodes.

VII. Conclusion

This paper has presented a simulation technique for steady-state free-running oscillator analysis. The theoretical basis of the algorithm was described, and it was implemented using the Fourier-transform-based harmonic balance method and the frequency-domain spectral balance arithmetic operator method for nonlinear analysis. The oscillator analysis technique was used to simulate the output power and oscillation frequency of a GaAs MMIC varactor-tuned FET oscillator. Good agreement between simulated and measured oscillator characteristics was obtained.

Acknowledgment

The design, fabrication, and experimental characterization of the voltage-controlled oscillator are largely due to the talents of D. Zimmerman, J. Culver, M. Smith, K. Anderson, T. Pavio, J. Beall, D. Zych, and J. Vaillan Court of Texas Instruments. The authors are grateful to the reviewer who pointed out that including $\mathrm{Re}\{Y_1\} = 0$ in the augmented set of equations (originally only $\mathrm{Im}\{Y_1\} = 0$ was included) would improve convergence in certain situations.

References

[1] M. Maeda, K. Kimura, and H. Kodera, "Design and performance of X-band oscillators with GaAs Schottky-gate field-effect transistors," *IEEE Trans. Microwave Theory Tech.*, vol. MTT-23, pp. 661–667, Aug. 1975.

[2] S. Hamilton, "Microwave oscillator circuits," *Microwave J.*, vol. 21, pp. 63–84, Apr. 1978.
[3] R. J. Trew, "Design theory for broad-band YIG-tuned FET oscillators," *IEEE Trans. Microwave Theory Tech.*, vol. MTT-27, pp. 8–14, Jan. 1979.
[4] V. Rizzoli, A. Lipparini, and E. Marazzi, "A general-purpose program for nonlinear microwave circuit design," *IEEE Trans. Microwave Theory Tech.*, vol. MTT-31, pp. 762–770, Sept. 1983.
[5] V. Rizzoli and A. Neri, "A fast Newton algorithm for the analysis and design of microwave oscillators and VCOs," in *Proc. 19th European Microwave Conf.*, Sept. 1989, pp. 386–391.
[6] Microwave Harmonica, Compact Software Inc., Paterson, NJ.
[7] Y. Wang and K. Gu, "Modeling, analysis and optimization of Gunn diode VCO," in *1990 IEEE MTT-S Int. Microwave Symp. Dig.*, May 1990, pp. 327–330.
[8] J. M. Paillot, *et al.*, "A general program for steady state, stability, and FM noise analysis of microwave oscillators," in *1990 IEEE MTT-S Int. Microwave Symp. Dig.*, May 1990, pp. 1287–1290.
[9] R. J. Gilmore and M. B. Steer, "Nonlinear circuit analysis using the method of harmonic balance—A review of the art," *Microwave and Millimeter Wave Computer Aided Eng.*, vol. 1. Part 1. Introductory concepts, no. 1, pp. 22–37; Part 2. Advanced concepts, no. 2, pp. 159–180, 1991.
[10] F. Sterzer, "Analysis of GaAs tunnel diode oscillators," *IEEE Trans. Electron Devices*, vol. ED-12, pp. 242–245, May 1965.
[11] K. Kurokawa, "Some basic characteristics of broadband negative resistance oscillator circuits," *Bell Syst. Tech. J.*, vol. 48, pp. 1937–1955, July 1969.
[12] K. Solbach, "Simulation study of harmonic oscillators," *IEEE Trans. Microwave Theory Tech.*, vol. MTT-30, pp. 1233–1237, Aug. 1982.
[13] B. D. Bates, "A comparison of IMPATT oscillator power and frequency above 100 GHz with results derived from theoretical models," *IEEE Trans. Microwave Theory Tech.*, vol. MTT-32, pp. 1394–1398, Oct. 1984.
[14] B. D. Bates and P. J. Khan, "Stability of multifrequency negative-resistance oscillators," *IEEE Trans. Microwave Theory Tech.*, vol. MTT-32, pp. 1310–1318, Oct. 1984.
[15] L. Gustafsson, G. H. B. Hansson, and K. I. Lundström, "On the use of describing functions in the study of nonlinear active microwave circuits," *IEEE Trans. Microwave Theory Tech.*, vol. MTT-20, pp. 402–409, June 1972.
[16] J. Xu and S. Li, "A feedback model of millimeter wave harmonic oscillators and its application," *Int. J. Infrared and Millimeter Waves*, vol. 10, pp. 1093–1101, Sept. 1989.
[17] L. O. Chua and Y. S. Tang, "Nonlinear oscillation via Volterra series," *IEEE Trans. Circuits Syst.*, vol. CAS-29, pp. 150–168, Mar. 1982.
[18] T. Endo and L. O. Chua, "Quasi-periodic oscillation via Volterra series," in *1986 IEEE Int. Symp. Circuits Syst. Dig.*, May 1986, pp. 57–60.
[19] Y. Hu, J. Obregon, and J. C. Mollier, "Nonlinear analysis of microwave FET oscillators using Volterra series," *IEEE Trans. Microwave Theory Tech.*, vol. 37, pp. 1689–1693, Nov. 1989.
[20] M. Fliess and F. Lamnabhi-Lagarrigue, "Application of a new functional expansion to the cubic anharmonic oscillator," *J. Math. Phys.*, vol. 23, pp. 495–502, Apr. 1982.
[21] K. K. M. Cheng and J. K. A. Everard, "A new and efficient approach to the analysis and design of GaAs MESFET microwave oscillators," in *1990 IEEE MTT-S Int. Microwave Symp. Dig.*, May 1990, pp. 1283–1286.
[22] Microwave Design System, Hewlett-Packard, Santa Rosa, CA.
[23] L. W. Nagel and D. O. Pederson, "SPICE (Simulation Program with Integrated Circuit Emphasis)," Memorandum ERL-M382, University of California, Electronics Research Laboratory, Apr. 1973.
[24] D. A. Warren, J. M. Golio, and W. L. Seely, "Large and small signal oscillator analysis," *Microwave J.*, pp. 229–246, May 1989.
[25] T. J. Brazil and S. O. Scanlan, "Self-consistent solutions for IMPATT diode networks," *IEEE Trans. Microwave Theory Tech.*, vol. MTT-29, pp. 26–32, Jan. 1981.
[26] D. Lippens, J.-L. Nieruchalski, and E. Constant, "Simplified particle simulation of millimeter-wave IMPATT devices," *IEEE Trans. Electron Devices*, vol. ED-32, pp. 2269–2276, Nov. 1985.
[27] P. A. Blakey, R. A. Giblin, and A. J. Seeds, "Large-signal time-domain modeling of avalanche diodes," *IEEE Trans. Electron Devices*, vol. Ed-26, pp. 1718–1728, Nov. 1979.
[28] C. R. Chang, M. B. Steer, and G. W. Rhyne, "Frequency-domain spectral balance using the arithmetic operator method," *IEEE Trans. Microwave Theory Tech.*, vol. 37, pp. 1681–1688, Nov. 1989.
[29] J. E. Dennis and R. B. Schnabel, *Numerical Methods for Nonlinear Equations and Unconstrained Optimization*. Englewood Cliffs, NJ: Prentice-Hall, 1983.
[30] P. L. Heron, C. R. Chang, and M. B. Steer, "Control of aliasing in the harmonic balance simulation of nonlinear microwave circuits," in *1989 IEEE MTT-S Int. Microwave Symp. Dig.*, vol. 1, pp. 355–358.
[31] E. Reese, Jr. and J. M. Beall, "Optimized X&Ku band GaAs MMIC varactor tuned FET oscillators," in *1988 IEEE MTT-S Int. Microwave Symp. Dig.*, May 1988, pp. 487–490.
[32] W. R. Curtice, "GaAs MESFET modeling and nonlinear CAD," *IEEE Trans. Microwave Theory Tech.*, vol. 36, pp. 220–230, Feb. 1988.
[33] C. R. Chang and M. B. Steer, "Frequency-domain nonlinear microwave circuit simulation using the arithmetic operator method," *IEEE Trans. Microwave Theory Tech.*, vol. 38, Aug. 1990.
[34] K. S. Kundert and A. Sangiovanni-Vincentelli, "Simulation of nonlinear circuits in the frequency domain," *IEEE J. Selected Areas Commun.*, vol. SAC-2, pp. 521–535, Jan. 1984.
[35] R. Gilmore, J. Gerber, M. Eron, and M. Anton, "Nonlinear design of MMICs using a microwave design workstation," *Microwave and RF Eng.*, pp. 43–50, June/July 1989.
[36] R. Gilmore, J. Gerber, M. Eron, and M. Anton, "New design workstation simplifies the design process," *Microwave J.*, pp. 138–146, July 1989.

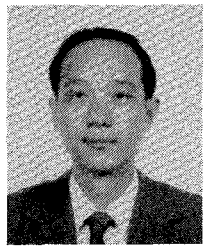

Chao-Ren Chang received the B.S. degree from National Cheng Kung University, Taiwan, Republic of China, in 1971 and the M.S. and Ph.D. degrees from North Carolina State University in 1980 and 1990, all in electrical engineering.

From 1976 to 1979 and from 1981 to 1984, he was an assistant scientist in the Microwave Laboratory of the Chung Shan Institute of Science and Technology, Taiwan. From 1984 to 1990 he was a teaching and research assistant at North Carolina State University, Raleigh. He is currently a Senior Microwave Engineer at Compact Software, Paterson, NJ. His research interests are in computer-aided analysis, the design and testing of nonlinear microwave circuits, and the characterization of microwave devices.

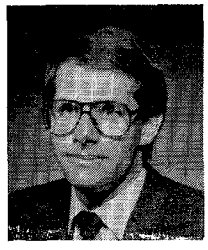

Michael B. Steer (S'78–M'82–SM'90) received the B.E. and Ph.D. degrees in electrical engineering from the University of Queensland, Brisbane, Australia, in 1978 and 1983 respectively. He joined North Carolina State University in 1983, where he is now an Associate Professor of Electrical and Computer Engineering.

His research involves the simulation and computer aided design of high-speed digital systems and of nonlinear microwave circuits and systems. He is currently working on the simulation of microwave analog circuits, high-speed printed circuit boards and multichip modules, on parameter extraction and computer-aided design of microwave and digital circuits using simulated annealing, and on millimeter-wave quasi-optical techniques. He presents a course at the National Technological University entitled "Computer Aided Circuit Analysis" which is broadcast throughout the U.S.

Dr. Steer has published more than 25 journal papers on nonlinear microwave circuit analysis, high-speed digital system simulation, simulation of delta–sigma modulators, high frequency limits of transistors,

microwave measurements, and equivalent circuits of diode mounts. He is active in the IEEE Microwave Theory and Techniques Society. In 1987 he was named a Presidential Young Investigator.

Scott Martin received the B.S. and the M.S. degrees in electrical engineering from Texas A&M University in 1986 and 1987, respectively.

In 1988 he joined the Microwave Laboratory at Texas Instruments. At TI he has designed hybrid and monolithic amplifiers and VCO's from S-band through Q-band.

Elias Reese, Jr. (S'81–M'81) received the B.S.E.E. degree from the University of Texas at Austin and the M.S.E.E. degree from Stanford University.

From 1981 through 1985, he was a member of the Signal Analysis Division Research and Development Laboratory at the Hewlett-Packard Company. There his work included microwave receiver component development, magnetic field modeling, and the development of tunable sources and filters using ferrite materials. In 1985, he joined the Microwave Laboratory at Texas Instruments, where he has pursued MMIC modeling and design. His work at Texas Instruments has included monolithic VCO development from S through Q band, as well as power amplifier, low-noise amplifier, mixer, switch, attenuator, and phase shifter MMIC development through Ku band. Currently, he leads the MMIC modeling and CAD section of the GaAs Electronics Department.